Arabian Journal of Geosciences (2018) 11: 3
https://doi.org/10.1007/s12517-017-3349-6

ORIGINAL PAPER

Hydrochemical, isotopic, and reservoir characterization of the Pasinler (Erzurum) geothermal field, eastern Turkey

Esra Hatipoğlu Temizel[1] · Fatma Gültekin[1]

Received: 23 September 2016 / Accepted: 12 December 2017 / Published online: 29 December 2017

Abstract

The reservoir temperature and conceptual model of the Pasinler geothermal area, which is one of the most important geothermal areas in Eastern Anatolia, are determined by considering its hydrogeochemical and isotope properties. The geothermal waters have a temperature of 51 °C in the geothermal wells and are of Na–Cl–HCO_3 type. The isotope contents of geothermal waters indicate that they are of meteoric origin and that they recharge on higher elevations than cold waters. The geothermal waters are of immature water class and their reservoir temperatures are calculated as 122–155 °C, and their cold water mixture rate is calculated as 32%. According to the $\delta^{13}C_{VPDB}$ values, the carbon in the geothermal waters originated from the dissolved carbon in the groundwaters and mantle-based CO_2 gases. According to the $\delta^{34}S_{CDT}$ values, the sources of sulfur in the geothermal waters are volcanic sulfur, oil and coal, and limestones. The sources of the major ions (Na^+, Ca^{2+}, Mg^{2+}, Cl^-, and HCO_3^-) in the geothermal waters are ion exchange and plagioclase and silicate weathering. It is determined that the volcanic rocks in the area have effects on the water chemistry and elements like Zn, Rb, Sr, and Ba originated from the rhyolite, rhyolitic tuff, and basalts. The rare earth element (REE) content of the geothermal waters is low, and according to the normalized REE diagrams, the light REE are getting depleted and heavy REE are getting enriched. The positive Eu and negative Ce anomalies of waters indicate oxygen-rich environments.

Keywords Pasinler geothermal area · Hydrogeochemistry · Isotope geochemistry · Water–rock interaction · Conceptual model · Erzurum, Turkey

Introduction

Turkey is located in volcanic regions and active earthquake lines; thus, it is very rich in geothermal waters. The number of thermal sources is more than 1500, but about 200 of them are operated as spas. Despite the high potential of the sources, the spa tourism in Turkey is only regional.

Geothermal areas in Turkey are investigated intensively along the grabens at Western Anatolia (Filiz 1982; Simsek 1982; Gülec 1988; Simsek 1997; Gemici and Filiz 2001; Yılmazer 2001; Tarcan 2002; Tarcan and Gemici 2003; Tarcan 2005; Magri et al. 2010; Karakus and Simsek 2013; Bundschuh et al. 2013), the Northern Anatolian fault zone, and Central (Gultekin et al. 2011; Baba and Sanliyuksel 2011; Pasvanoglu and Gultekin 2012). But, there are very few geothermal studies in the Eastern Anatolian volcanic region (Pasvanoğlu 2013; Yüce and Taskıran 2013; Firat Ersoy and Calik Sönmez 2014).

Pasinler, located 40 km to the east of Erzurum City, is one of the geothermal fields in Eastern Anatolia, which is a volcanic and neotectonic province of Turkey (Fig. 1). The study area has a semiarid climate and annual mean air temperature is 5.5 °C. The average annual precipitation is 474.6 mm, and the mean evapotranspiration is 543.9 mm in the region. The main surface waters in the study area are the Hasankale River (HC) and the Hamam Stream (HD). Jandarma spring (JK) is the most important cold spring in the basin (Fig. 2).

Many geothermal springs are present and seven geothermal wells having depths of 200–750 m have been drilled by MTA (General Directorate of Mineral Research and Exploration of Turkey) to develop the geothermal energy production in the Pasinler geothermal field. Although the geothermal wells (PS1-A, PS-2, PS-3, PS-4, PS-5, EHD-1, OZ) have a

✉ Esra Hatipoğlu Temizel
hatipogluesra@gmail.com

[1] Department of Geological Engineering, Karadeniz Technical University, 61080 Trabzon, Turkey

temperature 22.5 to 51 °C, people have been using the thermal waters in this area only for balneotherapy and bathing purposes. Because of their temperature, however, most of these waters can also be used for different purposes such as greenhouse irrigation, barn and poultry heating, mushroom cultivation, soil heating, swimming pools, and fish farms (Lund et al. 2010).

Geochemical studies of geothermal systems provide a framework to understand the physiochemical processes responsible for their origin and evolution. In addition, hydrogeochemical studies have a great importance in determining the intended use of water. The aims of this study are to investigate the hydrochemical properties and the source of hot waters in the Pasinler geothermal area, define the hot water transportation system, and determine the reservoir temperatures. As can be seen from the above explanations, in the Pasinler geothermal field, detailed hydrogeochemical studies have not been done yet. These deficiencies will be eliminated with this study.

Materials and methods

Between 2011 and 2012, fieldwork was carried out four times in the surroundings of Pasinler (Erzurum) in order to collect water samples from boreholes, springs, streams, and shallow cold groundwater systems, for chemical and isotopic ($\delta^{18}O$,

Fig. 1 Location map of the Pasinler geothermal field (Erzurum, Turkey)

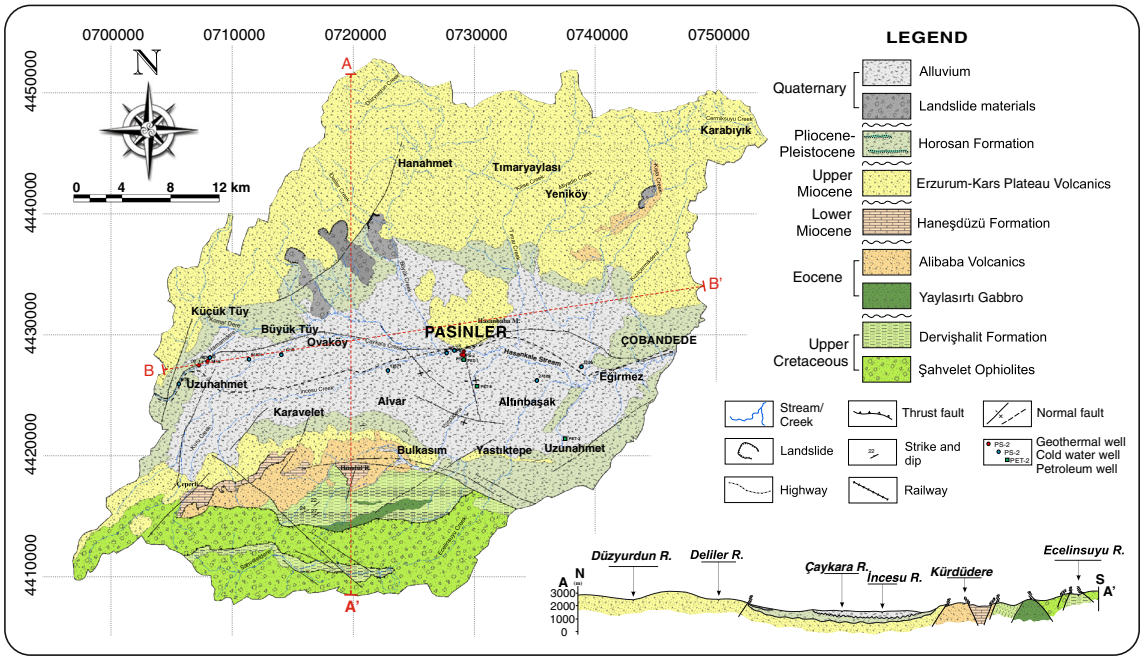

Fig. 2 Geological map of the Pasinler geothermal field (revised from Yılmaz et al. 1989) and geological cross section of the Pasinler geothermal field

δ^2H, tritium, δ^{13}C, δ^{34}S) analyses. Total dissolved solids (TDS), electrical conductivity (EC), pH, and water temperature (*T*) were measured in situ by using a portable multiparameter (YSI). Samples were collected in 250- and 100-mL polyethylene bottles which had been rinsed with distilled water twice before sampling for anion–cation and trace element analyses respectively. Double-capped polyethylene bottles with 100 mL (δ^{18}O, δ^2H, δ^{13}C) and 500 mL (^{3}H and δ^{34}S) volume were used for isotope samples. Major anion and cation compositions of the water samples were determined at the Water Chemistry Laboratory at Hacettepe University (Turkey), using the following methods: Major cations (Ca^{2+}, Mg^{2+}, Na^+, and K^+) were analyzed by ion chromatography system. Cl^- was analyzed using an $AgNO_3$ titrimetric method. Sulfate concentrations were determined by spectrophotometry together with alkalinity standard titration methods, whereas B and SiO_2 were analyzed with the spectrophotometric method. The major ion balance error of analyses is less than 5%. Heavy metal and rare earth element (REE) concentrations were analyzed at the ACME Laboratory (Canada) using inductively coupled plasma mass spectrometry (ICP/MS). In this study, the geothermal water analyses of the MTA (Akkus et al. 2005) were utilized for water chemistry study. Water chemistry analyses were applied according to the American Public Health Association (APHA 1995), American Water Works Association (AWWA 1995), and Water Pollution Control Federation (WPCF 1995) standards. δ^{18}O, δ^2H, δ^{13}C, and δ^{34}S isotopic analyses were done at the ISO Analytical Laboratory in the UK using equilibration IRMS (isotope ratio mass spectrometry) and acid-CF-IRMS methods. Results are reported in per mille vs. V-SMOW (Vienna-Standard Mean Ocean Water), V-PDB (Vienna–Peedee Belemnite), and V-CDT (Vienna Canyon Diablo Troilite) standards. ^{3}H was analyzed by a liquid scintillation water chemistry laboratory at Hacettepe University (Ankara). Tritium is reported in tritium units (TU) with a total analytical error of 0.1 to 0.3 TU.

Table 1 Lithostratigraphic relations of the geologic units and hydrogeological properties

Age	Formation	Lithology	Hydrogeological properties
Quaternary		Alluvium	Permeable
Pliocene–Pleistocene	Horosan formation	Conglomerate, sandstone, marl, siltstone claystone	Semipermeable
Upper Miocene	Erzurum-Kars plateau volcanics	Andesite, basalt, dacite, rhyodacites, rhyolite, and pyroclastics	Permeable (pyroclastics), semipermeable (volcanic rocks)
Lower Miocene	Haneşdüzü formation	Reef limestones, sandstone, claystone conglomerate	Semipermeable
Eocene	Alibaba volcanics	Andesite, basalt, pyroclastics	Impermeable
Eocene	Yaylasırtı gabbros	Gabbros	Impermeable
Eocene	Derviş Halit formation	Shale, claystone, marl, sandstone, and sandy limestones	Impermeable (shale, claystone, marl), permeable (sandstone)
Upper Cretaceous	Şahvelet ophiolites	Serpentinite, peridotite, gabbro, and diabase	Impermeable

Table 2 Results of physical and chemical analyses of the waters from the study area

Sample name	Description	Date of sampling	*T* (°C)	pH	EC (μS/cm)	TDS	Ca	Mg	Na	K	HCO_3	SO_4	Cl	SiO_2	Facies
PS1-A	Borehole	Aug. 1991[a]	42	7.6	4060	2639	104	73	570	41	1202	16	628	170	
PS-2	Borehole	Aug. 1991[a]	42	7.5	5641	3667	69	104	920	74	1530	5	1059	169	
		Oct. 1994[a]	40	7.01	5030	3270	150	76	850	60	1410	5.7	1040		
		May 2011	37	5.3	6330	4115	219	93	890	83.7	1670	5.2	1155	172	Na–Cl–HCO_3
		May 2012	38.4	5.2	5692	3700	200	100	910	86.8	1625	5.7	1174	170	Na–Cl–HCO_3
PS-3	Borehole	May 2012	36.9	5.5	6516	4236	240	89	910	73.7	1830	3.04	1078	171	Na–Cl–HCO_3
		Aug. 2012	36	6.5	6274	4392	245	106	927	72.2	1920	3.16	1060	173	Na–HCO_3–Cl
		Nov. 2012	37.6	6.5	6621	4304	241	105	895	71.2	1910	2.88	1074	172	Na–Cl–HCO_3
PS-4	Borehole	Aug. 2000[a]	42	6.7	6604	4293	185	75	1005	70	1930	3.9	1020		
		May 2011	36.1	5.1	5505	3637	201	83.3	1010	77.5	1910	4.2	1970	157	Na–HCO_3–Cl
PS-5	Borehole	Aug. 2000[a]	39	6.1	5120	3584	163	81.9	700	81.2	1571	6.6	976		
HDK	Thermal spring	May 2011	34.4	6.3	5243	3408	293	198	361	51.5	1925	1.1	578	190	Mg–Na–Ca–HCO_3–Cl
		May 2012	34.2	6.3	4844	3149	289	159	354	42.9	1817	0.51	475	181	Na–Ca–Mg–HCO_3–Cl
		Aug. 2012	34	6.5	5404	3513	286	161	405	42.1	1919	0.34	535	174	Na–Ca–Mg–HCO_3–Cl
		Nov. 2012	33.6	6.5	4810	3367	281	165	410	42.1	1921	0.33	540		Na–Ca–Mg–HCO_3–Cl
OZ	Borehole	May 2011	23	6.2	1456	946	93.7	58.3	59.2	10.3	700	1.2	24	125	Mg–Ca–Na–HCO_3
		May 2012	23.1	6.2	1457	930	99	60.1	59.1	10	730	1.41	20	160	Mg–Ca–Na–HCO_3
		Aug. 2012	23	6.2	1506	1014	100	61.3	59.3	10	760	1.24	20	123	Mg–Ca–HCO_3
		Nov. 2012	22.5	6.4	1529	990	101	61.6	57.5	9.63	731	5.04	21		Mg–Ca–HCO_3
JK	Cold spring	May 2012	13.3	7.8	420	304	33	23	11.3	2.66	221	7.8	2.02		Mg–Ca–HCO_3
		Aug. 2012	14.2	7.9	470	308	35.8	22.1	11	2.33	223	7.3	2.18		Mg–Ca–HCO_3
		Nov. 2012	13.2	7.9	504	328	38	22.5	13.8	3.43	225	7.27	11.1		Ca–Mg–HCO_3
HC	Stream water	May 2012	18.4	6.3	452	293	40	18	10	3.2	208	7.4	4		Ca–Mg–HCO_3
		Aug. 2012	23.1	7.7	721	505	63	33	20	5.1	346	18	7.5		Ca–Mg–HCO_3
		Nov. 2012	9.6	8.2	784	510	60	26	19.5	5.4	371	9.7	9.8		Ca–Mg–HCO_3
HD	Stream water	May 2012	18.7	6.3	1142	742	86	48	35.2	7.1	545	4.24	15		Ca–Mg–HCO_3
		Aug. 2012	19.8	7.4	1122	785	85	47.2	40.6	7.2	582	3.76	17.9		Ca–Mg–HCO_3
		Nov. 2012	11.9	6.9	1013	709	82	45.9	38.4	6.7	512	4.07	16.3		Ca–Mg–HCO_3
HDE	Stream water	May 2012	11.7	6.1	810	525	70	37.3	12.9	2.5	389	6.25	6.5		Ca–Mg–HCO_3
		Aug. 2012	20.9	7.9	750	523	70.8	36.7	11.5	4.3	383	7.11	6.2		Ca–Mg–HCO_3
		Nov. 2012	8.4	8.6	710	461	62.3	32.4	10.4	3.2	335	8.1	5.45		Ca–Mg–HCO_3
3205		Jun. 2011[b]	14.8	8.02	475	310	12	8.4	60	2.34	189	0.48	36.2		
		Sept. 2012[b]	13.1	7.9	394	275	24.4	17	52.2	7	129	0.48	30		Na–Mg–Ca–HCO_3
11216		Jun. 2009[b]	16.3	8.07	310	202	18	14.4	10.3	3.1	152	2.4	0.71		
		Oct. 2009[b]	16	7.9	342	223	28	10.8	11.5	3.51	152	9.12	7.1		
12571		Jun. 2011[b]	15.5	7.9	273	180	15.2	10.3	13.1	3.9	128	2.4	7.1		
		Sept. 2012[b]	14.1	8.01	308	200	27.4	18.3	14.7	1.95	110	9.6	6		Mg–Ca–Na–HCO_3
27335		Jun. 2011[b]	13.3	7.8	305	196	14	10.3	24.6	1.5	116	17.7	12.7		
		Sept. 2012[b]	14	8.06	316	206	27.6	21.7	20.7	0.7	103	23	9.2		Mg–Ca–Na–HCO_3
54324		Jun. 2011[b]	13.9	7.3	300	195	18.4	10	14.2	7.8	134	1	8.5		
		Sept. 2012[b]	12.9	8.1	317	206	38.6	22.6	6.4	3.1	117	4.8	3.9		Mg–Ca–HCO_3

Cation and anion concentrations are in milligrams per liter

[a] Samples are results of analyses of MTA (Akkus et al. 2005)

[b] Samples from DSI (state hydraulic works)

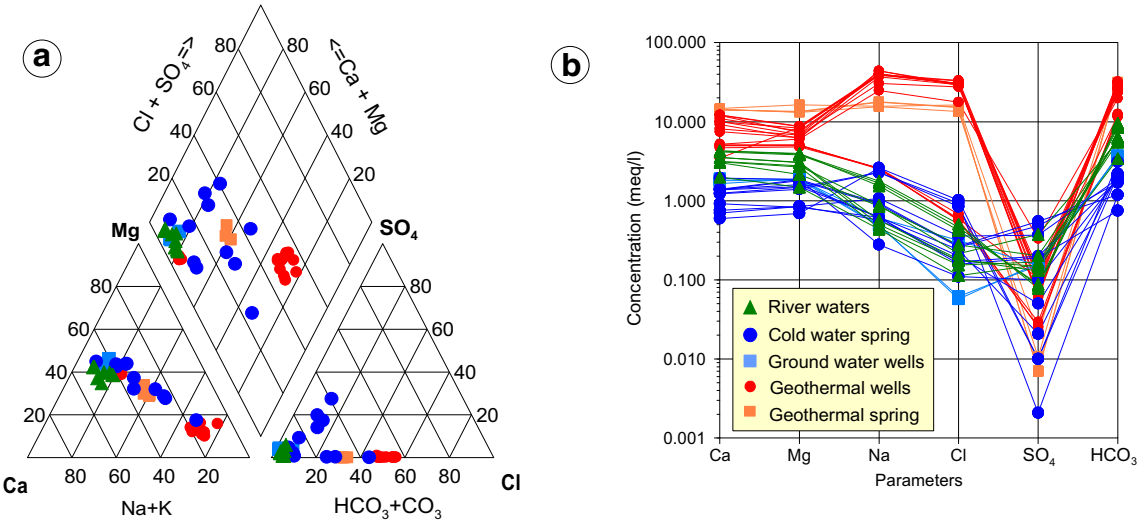

Fig. 3 Piper (**a**) and Schoeller (**b**) diagrams of the water samples

Saturation indexes of minerals were calculated by using the PHREEQC chemical equilibrium software WATEQ4F database (Parkhurst and Appelo 1999). The software AquaChem (Calmbach 1997) computer code was used to determine the hydrochemical properties of thermal and cold waters. Silica geothermometers were applied for reservoir temperature estimations to Pasinler geothermal waters. These methods are referred to Fournier (1977) and Arnorsson (1983) formulations.

Geological and hydrogeological settings

The dominant rock types in the Pasinler (Erzurum) geothermal area are volcanics that are formed at different times. These volcanics are overlain by young sediments and alluvium at the center of the area (Fig. 2). The basement rocks of the study area are Upper Cretaceous age Şahvelet ophiolites including serpentinite, peridotite, gabbro, and diabase (Yılmaz et al. 1989).The Şahvelet ophiolites are unconformably overlain by the Derviş Halit formation and Tertiary units (Fig. 2). The Derviş Halit formation comprises shale, claystone, marl, sandstone, and sandy limestones. Yaylasırtı gabbros of the Eocene age (Sungurlu 1971) are massive and display a fractured structure. Andesite, basalt, pyroclastics of Alibaba volcanics are (Sungurlu 1971) conformably overlain by Late Oligocene Early Miocene units. The Haneşdüzü formation of Lower Miocene age consists of reef limestones. Erzurum-Kars plateau volcanics of Upper Miocene age is formed andesite, basalt, dacite, rhyodacites, rhyolite, and pyroclastics. The Horosan formation (conglomerate, sandstone, marl, siltstone claystone) and Quaternary alluvium are the youngest units in the field.

In the study area which is one of the most neotectonic provinces of Turkey, strike–slip faults and intense fracture networks formed by the compressional tectonic regime are the basic structural elements (Şengör 1980). These structural elements have enhanced the development of the geothermal system and the circulation of the thermal waters.

The stratigraphic units are classified according to the hydrogeological characteristics of the rocks. According to the Bureau of Reclamation (1995) classification, alluviums and Erzurum-Kars plateau volcanics with a hydraulic conductivity value of 10^{-5} m/s (Dilek, 1973; Freeze and Cherry, 1979) are permeable units. The semipermeable units are Horosan formation and Haneşdüzü formation with 10^{-7} m/s (Dilek, 1973) hydraulic conductivity. The Şahvelet ophiolites, Derviş Halit formation, and Alibaba volcanics with permeability of about 10^{-10} m/s (Freeze and Cherry, 1979) are impermeable units (Table 1). A total of six geothermal wells (OZ, PS-2, PS-3, PS-4, PS-5, EHD-1), one geothermal spring (HDK), one cold water spring (JK), three surface waters (HD, HDE, HC), and five groundwater wells (3205, 11216, 12571, 27335, 54324) are evaluated in this study.

Results and discussion

Hydrogeochemistry

In order to conduct chemical analyses, samples were gathered from the geothermal wells and hot and cold water springs in the area. Also, the results of the analyses that were carried out by MTA on geothermal waters and by DSI (State Hydraulic Works) on cold waters were also assessed. The physicochemical characteristics and types of all waters are presented in Table 2. In the study area, the water temperature of hot spring

Table 3 Trace element compositions of the waters from the study area (μg/L)

	PS-2	PS-3	PS-4	HDK	OZ	JK	HC	HD	HDE
Al	10	23	10	20	2	1	20	24	10
As	20	22	17	20	0.5	6.7	6.3	23	5
B	9998	10,364	9042	14,700	1075	50	110	14,707	40
Ba	899	889	832	520	9.14	44.5	81.4	527	20
Br	1799	1726	1646	1700	175	10	10	1729	10
Cd	0.05	0.05	0.05	< 0.05	0.05	0.05	0.13	0.2	< 0.05
Co	0.02	0.02	0.02		0.02	0.02	0.11	0.29	
Cs	12.3	12.8	10.6		0.35	0.01	0.03	3.7	
Cu	1	1	1	0.5	0.3	0.2	2.6	3.2	0.5
Fe	4081	4257	3837	4300	4845	< 0.01	< 0.01	4305	< 0.01
Ga	0.05	0.05	0.05		0.05	0.05	0.05	0.05	
Ge	3	4.2	3	3	0.9	0.5	0.5	0.3	0.5
Hf	0.02	0.02	0.02		0.02	0.02	0.02	0.02	
Hg	< 1	< 1	< 1		0.2	0.1	0.1	0.2	
Li	1209	1227	1092	300	67.6	2	5	310	30
Mn	476	494	440	100	103	< 0.05	< 0.05	141	< 0.05
Mo	< 0.1	< 0.1	< 0.1		0.3	0.9	5.6	1.1	
Nb	0.2	0.2	0.2		0.01	0.01	0.02	0.01	
Ni	0.2	4	0.2	5	0.2	0.7	3.7	5	< 0.02
Pb	1	1	1	1	0.5	0.1	0.4	0.7	0.3
Rb	140	147	131	80	11.5	2.71	6.6	82.8	2
Sb	0.05	0.05	0.05		0.05	0.08		0.21	0.22
Sc	21	22	20	20	15	2	2	22	5
Se	6	5	5		0.7	0.5	1.2	5	
Si	80,803	80,103	73,522	89,100	58,941	10,000	12,600	89,130	21,800
Sn	0.05	0.05	0.05		0.13	0.05	0.07	0.08	
Sr	2366	2578	2370	2500	367	492	695	2520	300
Ta	0.02	0.02	0.02		0.02	0.02	0.02	0.02	
Th	0.05	0.05	0.05		0.09	0.05	0.05	0.05	
Tl	0.1	0.1	0.1		0.01	0.01	0.04	0.08	
U	0.02	0.02	0.02		0.02	0.6	2.16	0.57	
W	0.2	0.2	0.2		0.08	0.10	0.22	0.25	
Y	0.6	0.6	0.6		0.02	0.01	0.03	0.3	
Zn	7	10	5	8	1.9	4	15.5	10	1
Zr	1.7	2.2	2.9	0.2	0.03	0.02	0.04	0.05	0.2

waters ranges from 22.5 to 51 °C, and the pH values range from 5.7 to 7.6. The electrical conductivity (EC) values are in the range of 970–6233 μS/cm. The total dissolved solids (TDS) are between 2538 and 4392 mg/L. In contrast, the water temperatures of cold spring and river waters are ranging from 9.7 to 23.1 °C, and the pH values range from 6.15 to 8.6. Their TDS concentrations between 123 and 785 mg/L and EC ranged from 200 to 1142 μS/cm. Based on the International Association of Hydrogeologists (IAH 1979) classification, three different groundwater facies were determined (Table 2). Generally, geothermal wells are of Na–Cl–HCO_3 facies, geothermal springs are of Na–Ca–Mg–HCO_3–Cl facies, and cold waters are of Mg–Ca–HCO_3 facies. The main chemical characteristics of the studied waters are summarized in the Piper diagram in Fig. 3 (Piper 1944). The cold water and thermal well waters clearly plot in distinct fields. Hot spring waters are located between them. This situation indicates that the hot waters are mixed with shallow ground waters. According to the piper diagram, in the study area Ca–Mg–HCO_3 (stream waters, cold wells, cold spring and geothermal spring) and Na–Cl–HCO_3 (geothermal wells) the dominant water types were observed (Fig. 3a). The Schoeller diagram

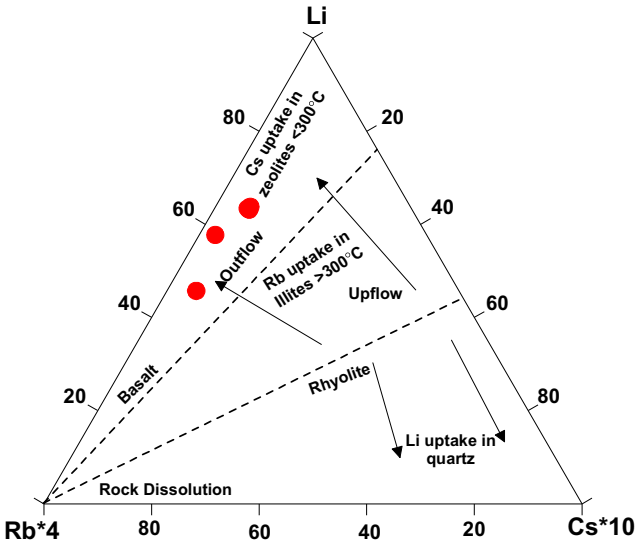

Fig. 4 Li–Rb–Cs diagram (symbol is as in Fig. 3b)

shows the total concentration of major ions in semi log-scale (Fig. 3b). As can be seen from this figure, thermal waters have different chemical characteristics to cold waters. While Na + K and Cl concentrations are high in the thermal waters, these values are low in cold waters. But the SO_4 concentration is low in all waters because of sulfate reduction. Sulfate is typically the first or second most abundant anion in natural waters (Hem, 1970). Sulfate is the completely oxidized form of sulfur, which is stable under aerobic conditions. Sulfate reduction occurs intensively in natural groundwater systems. In the studies on sulfate reduction, it has been stated that sulfate reduction makes a significant amount of H^+ consumption and HS^- production (Miao et al., 2012). In addition, sulfate reduction under natural conditions is conducted by prokaryotic bacteria through chemical reactions in which organic carbon or H_2 is oxidized while sulfate is reduced (Canfield 2001); sulfate-reducing bacteria are effective on the subsurface sulfate reduction (Berner et al., 2002; Aravena and Mayer, 2009). The most significant indicator of sulfate reduction is H_2S production (Miao et al., 2012). In the study area, an intense odor of rotten eggs around geothermal wells and thermal springs is an indication of H_2S production and sulfate reduction. The measured low pH and relatively high Fe concentration in the thermal water support this subject.

Trace element contents of waters

Trace elements like Li, B, Co, Ni, Ga, Rb, Cs, Sr, and Ba remain unaffected in the thermal waters due to secondary processes (Giggenbach 1991) and hence play a significant role in understating the evolution of the thermal waters. Plenty of trace elements in geothermal waters indicates that thermal waters have a greater reactivity leading to increased leaching of the minor elements from the host rock during deep circulation (Ma et al. 2011).Trace element analyses have been carried out on the samples taken from geothermal wells, hot–cold springs, and surface waters. Trace element concentrations of the Pasinler waters are presented in Table 3. The lithophile elements such as Li, Rb, and Cs, which are useful in understanding the deep processes (Giggenbach 1991), are plotted in the trilinear diagram (Fig. 4). All of the samples indicate uptake of Cs in zeolites at temperatures lower than 300 °C. The concentrations of these lithophile elements were in the range of 67.6–1227 ppb for Li, 0.35–12.8 ppb for Cs, and 11.5–147 ppb for Rb. Among the other lithophile elements, the concentrations of Sr and Ba in thermal waters are 367–2578 and 9.14–899 ppb, respectively. Sr, with higher concentrations than the other trace elements in the thermal water, reflects the interaction between the ascending thermal waters and volcanic rocks (Delalande et al. 2011). The boron concentration of the thermal waters varied from 1075 to 10,364 ppb. While the B concentration values in cold and surface waters are low (40–100 ppb), in the hot springs (HDK) discharging along the Hamam stream and stream water (HD), these values are high (14,700 ppb). The maximum Al and Mn abundances are 23 and 494.3 ppb, respectively, in the geothermal waters (Table 3). The chalcophile elements such as As, Cu, Pb, Se, and Zn are generally dominant in the sulfate waters. The concentration of these elements ranges in the Pasinler waters from 0.5 to 23 ppb for As, 0.3 to 1 ppb for Cu, 0.5 to 1 ppb for Pb, 0.7 to 6 ppb for Se, and 1.9 to 10 ppb for Zn. In the presence of sulfur species, the solubility of minerals containing chalcophile elements is lower in reducing conditions than in oxidizing conditions (Hem 1970). The concentrations of chalcophile elements are low in the investigated water due to sulfate reduction. Among the siderophile elements, the concentrations of Fe, Ni, and Ge in the waters are 3837–4845, 0.2–4, and 0.9–4.2 ppb, respectively. The concentrations of Hg and Mo ranged from below detection limit to 1 ppb Hg and 0.1 ppb Mo (except sample OZ). It was observed that thermal water had a good correlation between lithophile elements and chloride concentrations. Correlation coefficients computed for Cl–Li, Cl–Rb, Cl–Cs, Cl–Br, and Cl–B pairs are 0.939, 0.997, 0.961, 0.763, and 0.343, respectively (Fig. 5). A positive correlation was also observed between Rb, Li, and Cs themselves. Correlation coefficients calculated for these elements are 0.910 for Rb–Li, 0.939 for Rb–Cs, and 0.994 for Li–Cs. Strong correlations observed between K and Rb–Li–Cs (K–Rb 0.999, K–Cs 0.934, and K–Li 0.903) may indicate that these elements substitute for potassium in clay minerals (Mutlu 2007).

Geothermometers

Various chemical geothermometers have been developed to estimate the reservoir temperatures in the geothermal system (Arnorsson 1983; Fournier 1977, 1979; Giggenbach 1988; Kharaka and Mariner 1989; Truesdell and Fournier 1977; Verma and Santoyo 1997). Among these, the cation (Na–K, Na–Li, Na–K–Ca, etc.) and silica (quartz, chalcedony,

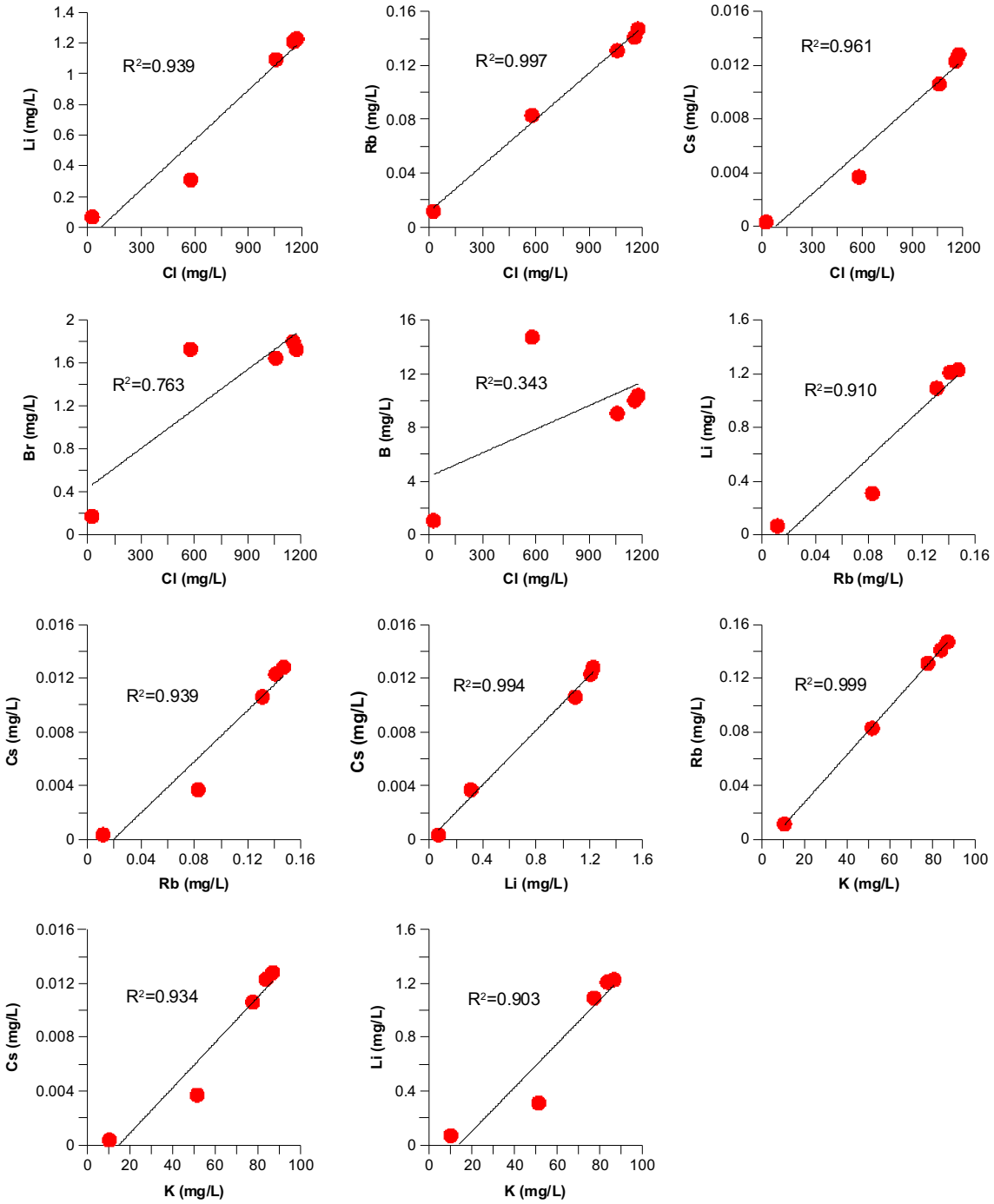

Fig. 5 Plots of Cl vs. Li, Cl vs. Rb, Cl vs. Cs, Cl vs. Br, Cl vs. B, Rb vs. Li, Rb vs. Cs, Li vs. Cs, K vs. Rb, K vs. Cs, and K vs. Li of all geothermal water samples (symbol is as in Fig. 3b)

amorphous silica, etc.) geothermometers are the most widely used. In this study, silica geothermometers were applied to calculate the reservoir temperatures of the thermal waters. The results of geothermometric calculations are given in Table 4, and the calculated reservoir temperature varies from 46 to 176.7 °C. Geothermometer results give a wide range for reservoir temperature. The reservoir temperatures of about 40–60 °C, calculated with amorphous silica and cristobalite thermometers, do not reflect the reality. Quartz geothermometers are not suitable for low temperatures (Fournier 1977). Therefore, the most reliable reservoir temperature for the Pasinler geothermal field is the temperatures of approximately 122–155 °C calculated by a chalcedony geothermometer. According to the Na–K–Mg diagram (Giggenbach 1988), Pasinler waters are located in the "immature

Table 4 Silica geothermometry temperatures for Pasinler thermal waters (°C)

Geothermometers	PS1A	PS-2	PS-3	PS-4	HDK	OZ
Surface temperature (°C)	42	37	36.9	36.1	34.4	23.03
1. SiO_2 (amorphous silica)[a]	46.1	47.1	46.6	41.5	53.2	28.9
2. SiO_2 (ά Kristobalit)[a]	119.1	120.2	119.6	113.9	126.8	100
3. SiO_2 (β Kristobalit)[a]	69.5	70.5	70	64.4	77.1	50.9
4. SiO_2 (chalcedony)[a]	146.4	147.7	147	140.7	155	125.3
5. SiO_2 (quartz)[a]	169.1	170.2	169.6	164.1	176.7	150.5
6. SiO_2 (quartz steam loss)[a]	159.3	160.2	159.7	155.2	165.5	143.8
7. SiO_2 (chalcedony conductive cooling)[b]	141.8	142.9	142.4	136.6	149.6	122.6
8. SiO_2 (quartz steam loss)[b]	137.3	138.2	137.7	132.8	144	120.6
9. SiO_2 (quartz steam loss)[b]	142	143.2	142.5	136.3	150.5	121.1
10. SiO_2 (quartz steam loss)[b]	162.9	164	163.4	157.4	171.1	142.6
11. SiO_2 (quartz steam loss)[b]	158.6	159.5	159	154.4	164.8	143

[a] Fournier (1977)

[b] Arnorsson et al. (1983)

waters" which indicates that these waters are shallow or mixed and, thus, have not yet reached the water rock equilibrium in the region (Fig. 6). For this reason, cation geothermometers give higher results and according to Giggenbach (1988) cannot be applied reliably.

Enthalpy–chloride mixing model

The enthalpy–chloride mixing model of Fournier (1977) was used to predict the underground temperature for the Pasinler mixed geothermal water. This mixing model takes into account both mixing and boiling processes (Magana 1999). Its application basically involves relating analyzed chloride levels to water enthalpy, which can be derived from measured discharge temperature, geothermometry temperature, and silica–enthalpy mixing model temperature (Magana 1999). Enthalpy–chloride and silica–enthalpy mixture models were applied to the Pasinler geothermal area, and reservoir temperatures are determined as 160–235 and 220–250 °C, respectively. But, when the geological properties of the basin are taken into account, it is considered that the temperature values that were calculated using the silica–enthalpy model are unrealistic. Thus, the reservoir temperatures that were calculated via the enthalpy–chloride model are accepted (Fig. 7). Moreover, the mixing ratio of hot water to the cold water supply was calculated as 32%. The thermal waters

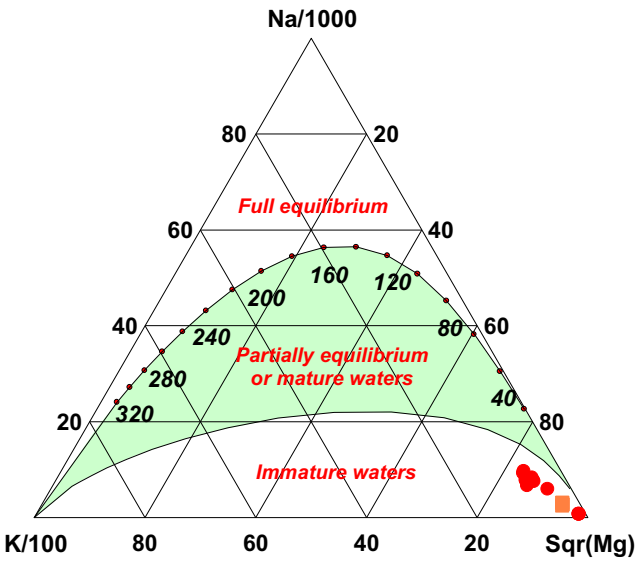

Fig. 6 Na, K, Mg trilinear equilibrium diagram (based on Giggenbach, 1988) for the geothermal water samples (symbols are as in Fig. 3b)

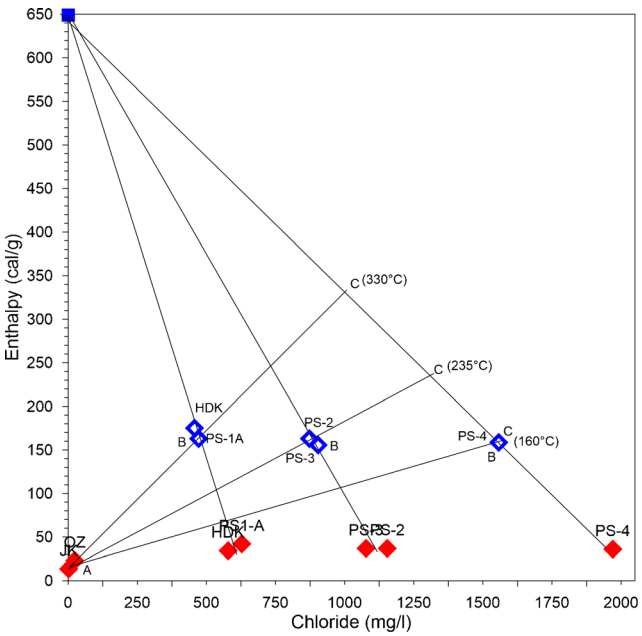

Fig. 7 Enthalpy-chloride mixing model for the Pasinler thermal waters

Table 5 Saturation index (SI) values of the waters in the study area

	PS1-A	PS-2	PS-3	PS-4	HDK	OZ	JK
Anhydrite	− 2.75	− 3.07	− 3.28	− 3.21	− 3.72	− 3.77	− 3.19
Aragonite	1.06	− 0.89	− 0.62	− 1.01	0.31	− 0.68	− 2.49
Barite	–	− 0.64	− 0.95	− 0.75	− 1.59	− 2.68	− 0.80
Calcite	1.20	− 0.75	− 0.49	− 0.87	0.45	− 0.53	− 2.34
Dolomite	2.75	− 1.40	− 0.92	− 1.65	1.19	− 0.94	− 4.65
Gypsum	− 2.62	− 2.92	− 3.12	− 3.05	− 3.55	− 3.55	− 2.94
Halite	− 5.14	− 4.71	− 4.73	− 4.69	− 5.38	− 7.45	− 9.17
Magnesite	0.96	− 1.24	− 1.03	− 1.38	0.15	− 0.99	− 2.85
Quartz	–	0.95	0.95	0.93	1.03	1.00	0.41
Talc	–	− 8.21	− 7.11	− 9.41	− 1.02	− 4.85	− 14.90
	HD	HDE	HC	3205	12,571	27,335	54,324
Anhydrite	− 3.22	− 3.06	− 3.12	− 5.17	− 3.14	− 2.71	− 3.32
Aragonite	− 0.74	− 1.25	− 2.45	0.13	− 0.24	0.15[d]	0
Barite	− 1.65	− 1.27	− 1.05	–	–	–	–
Calcite	− 0.59	− 1.09	− 2.30	0.28	− 0.08	0.30	0.15
Dolomite	− 1.17	− 2.31	− 4.69	0.62	− 0.15	0.70	0.24
Gypsum	− 2.98	− 2.81	− 2.88	− 4.92	− 2.89	− 2.46	− 3.07
Halite	− 7.86	− 8.62	− 8.94	− 7.30	− 8.60	− 8.22	− 9.13
Magnesite	− 1.14	− 1.75	− 2.95	− 0.21	− 0.61	− 0.15	− 0.45
Quartz	0.79	0.75	0.40	–	–	–	–
Talc	− 5.92	− 8.84	− 14.89	–	–	–	–

in the vicinity and the cold spring (JK) are close to the tritium values (0.03–0.57 TU). Therefore, the mixture is not with surface waters but with cold waters which are partly deep circulation.

Saturation indices

By using the saturation index approach, it is possible to predict reactive minerals in the subsurface from the groundwater chemical data without examining samples of the solid phases (Deutsch 1997).

Table 5 shows the saturation indices (SI) of the geothermal water from Pasinler calculated with the software PHREEQC Interactive 2.8 computer code WATEQ4F database (Parkhurst and Appelo 1999) on the basis of outlet temperature and pH. Results indicate that the studied geothermal wells (except the PS1-A) are supersaturated (SI > 0) with respect to quartz while they are undersaturated (SI < 0) with respect to anhydrite, aragonite, barite, calcite, dolomite, gypsum, halite, magnesite, and talc. The HDK hot spring is supersaturated with aragonite, calcite, dolomite, and quartz whereas it is undersaturated with anhydrite, barite, gypsum, halite, and talc (Fig. 8).

Isotopic characteristics

Isotope compositions of the waters have become important tools in hydrogeology and have been widely used as natural

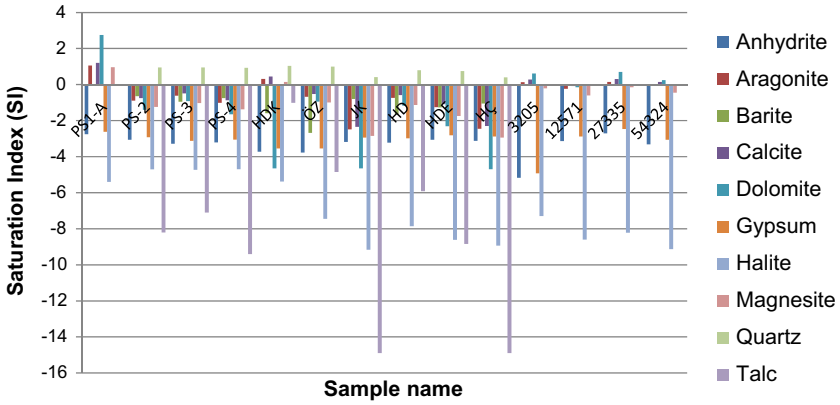

Fig. 8 Mineral equilibrium diagram for Pasinler thermal spring

Table 6 Isotopic analysis results of the water samples in the Pasinler geothermal area

Sample	Sampling date	$\delta D_{V\text{-}SMOW}$ (‰)	$\delta^{18}O_{V\text{-}SMOW}$ (‰)	T (TU)	$\delta^{13}C_{V\text{-}PDB}$ (‰)	$\delta^{18}O(SO_4)_{V\text{-}SMOW}$ (‰)	$\delta^{34}S(SO_4)_{V\text{-}CDT}$ (‰)
OZ	May 11	−94.68	−13.54	0.18			
OZ	May 12	−92.15	−13.32	0.0	9.18		
OZ	Aug. 12	−92.16	−13.35	0.61	9.34	−2.7	36.18
OZ	Nov. 12	−90.12	−13.24	0.0			
PS-2	May 11	−94.2	−13.37	0.33			
PS-3	May 11	−92.16	−13.4	0.0			
PS-3	May 12	−94.71	−13.3	0.57	8.8		
PS-3	Aug. 12	−93.44	−13.34	0.27	9.54	1.9	18.64
PS-3	Nov. 12	−96.05	−13.1	0.39			
HDK	May 12	−92.94	−13.01	0.28	8.13		
HDK	Aug. 12	−99.68	−12.95	0.75	9	6.1	31.35
HDK	Nov. 12	−91.2	−12.57	0.17			
JK	May 12	−84.87	−12.55	0.03	−9.99		
JK	Aug. 12	−86.71	−12.03	0.0	−7.14	5.4	1.94
JK	Nov. 12	−83.84	−12.19	0.0			
HD	May 12	−87.71	−12.65	2.49	3.22		
HD	Aug. 12	−94.1	−12.89	1.59	6.19	8	14.4
HD	Nov. 12	−88.95	−12.67	1.43			
HDE	May 12	−86.66	−12.34	3.76	−9.61		
HDE	Aug. 12	−90.73	−12.52	4.64	−7.93	3.8	13.44
HDE	Nov. 12	−87.15	−12.6	2.84			
HC	Aug. 12	−73.6	−11.55	5.46	−7.52		
HC	Nov. 12	−81.9	−11.64	6.83			

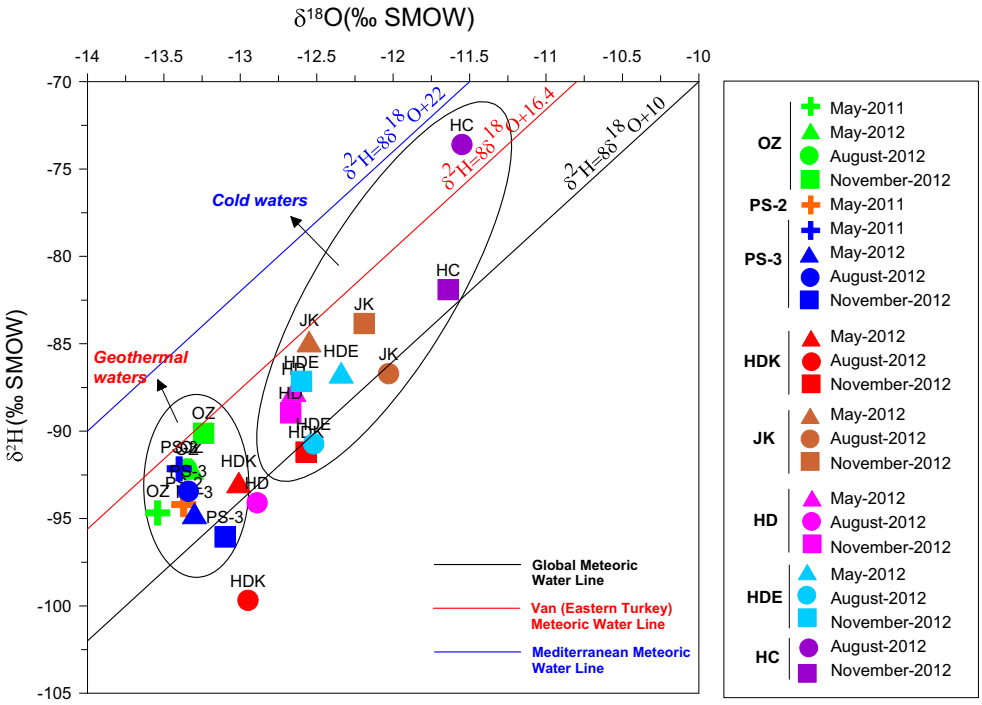

Fig. 9 Plot of δD vs. $\delta^{18}O$ of all water samples in the study area. The Mediterranean meteoric water line and the Van (Eastern Turkey) meteoric line are calculated from Gat and Carmi (1970) and Aydın et al. (2009), respectively

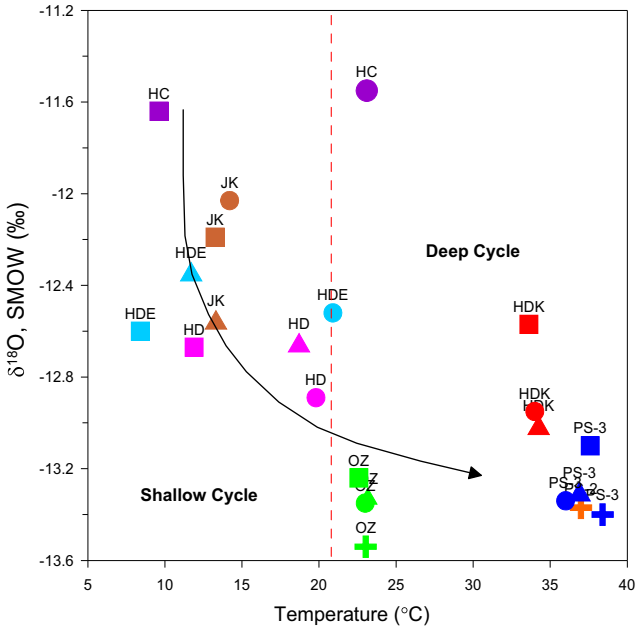

Fig. 10 Oxygen-18 ($\delta^{18}O$)–temperature diagram of the waters in the study area (symbols are as in Fig. 9)

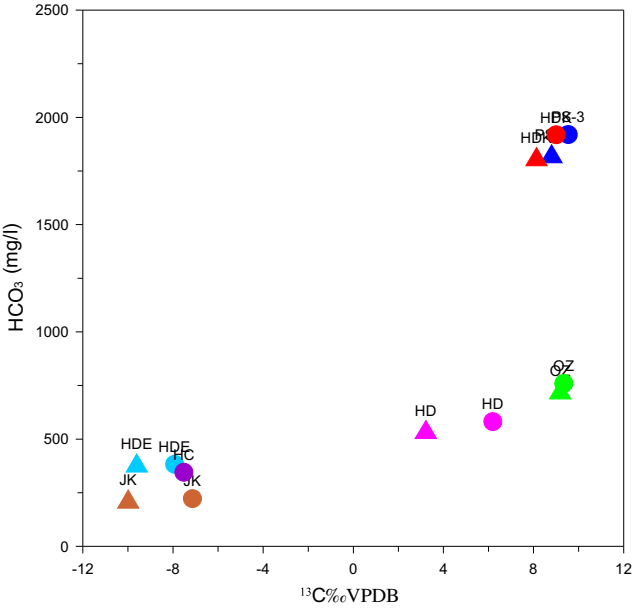

Fig. 12 HCO_3–$\delta^{13}C$ relation for the thermal and cold waters (symbols are as in Fig. 9)

tracers (Clark and Fritz 1997). All water samples were analyzed for $\delta^{18}O$, $\delta^{2}H$, and ^{3}H. Moreover, $\delta^{13}C$, $\delta^{34}S$, and $\delta^{18}O_{SO4}$ in DIC and dissolved sulfate have been performed on selected samples (Table 6). For thermal waters (spring and boreholes), the values of $\delta^{18}O$ range from −13.54 to −12.57‰ and those of $\delta^{2}H$ from −99.68 to −91.2‰. The $\delta^{2}H$ and $\delta^{18}O$ values of cold springs and river water samples vary from −90.73 to −73.6‰ and −12.89 to −11.55 ‰, respectively, and are similar to those for hot spring water samples. The stable isotopic composition ($\delta^{2}H$ versus $\delta^{18}O$) of the waters, both cold and thermal, is shown in Fig. 9. According to this diagram, the isotopic composition all of the waters in the study area is located between the Global Meteoric Water Line (GMWL) (Craig 1961) and the Mediterranean Meteoric

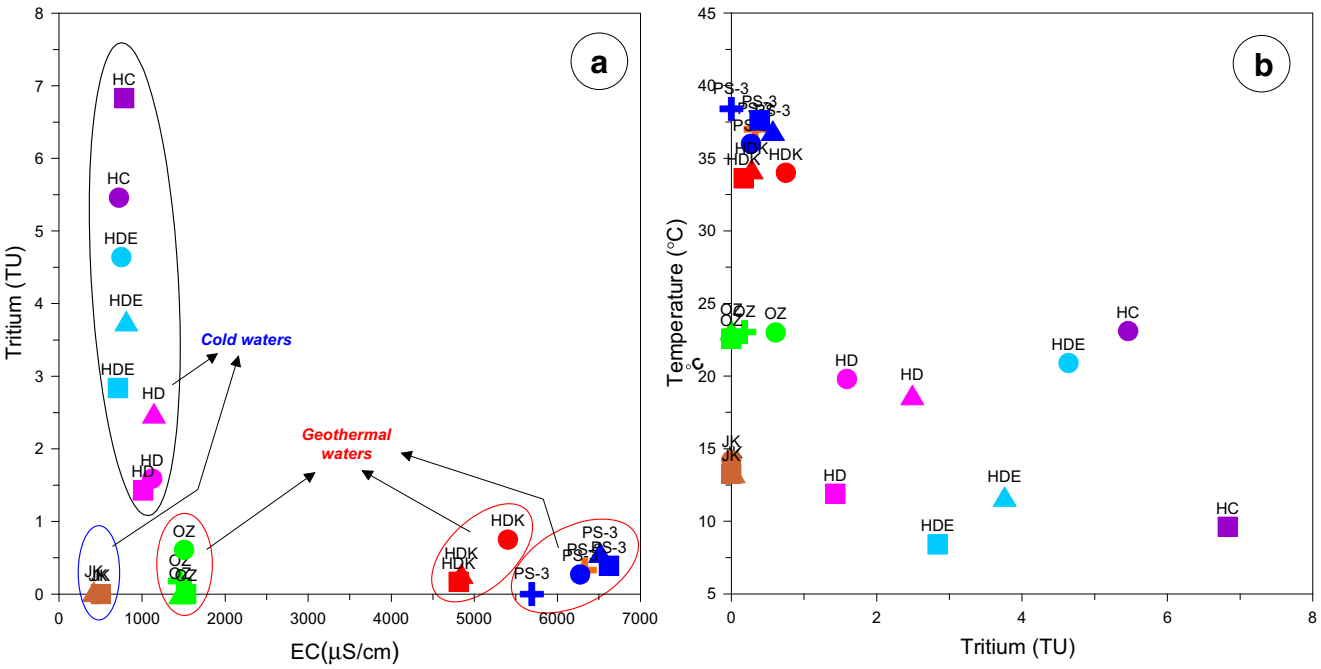

Fig. 11 Tritium–electrical conductivity (**a**) and tritium–temperature (**b**) relations for the thermal and cold waters (symbols are as in Fig. 9)

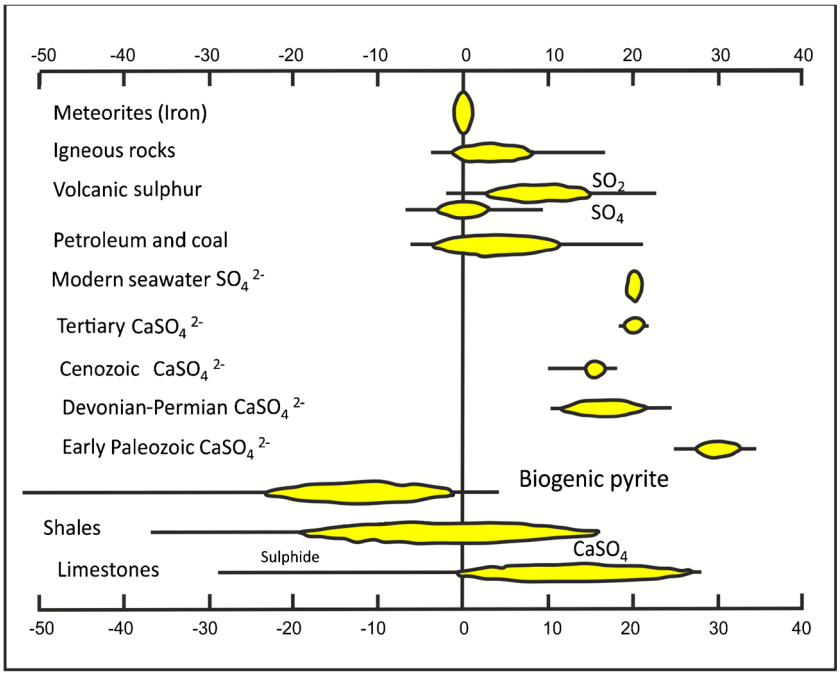

Fig. 13 $^{34}S_{CDT}$ values of sulfur in different material and environment (Krouse, 1980)

Water Line (Gat and Carmi 1970), and on the Van (East Turkey) Meteoric Line ($\delta^2H = 8\delta^{18}O + 16.4$; Aydın et al. 2009). This result indicates that the precipitations which feed the water sources are occurring in a more arid area than the world average (Fontes 1980). According to the Oxygen-18 vs. temperature diagram, thermal water samples were recharged at the same elevation in the basin (Fig. 10). Thermal waters in the field have more negative δ^2H and $\delta^{18}O$ values than cold waters. These low values indicate that thermal waters recharged at the higher altitude than cold waters.

Tritium contents of thermal waters and cold waters vary from 0.01 ± 0.50 TU to 6.83 ± 0.45 TU (Table 6). The amount of tritium in water can be used to qualitatively determine whether groundwater is modern or not (Clark and Fritz 1997;

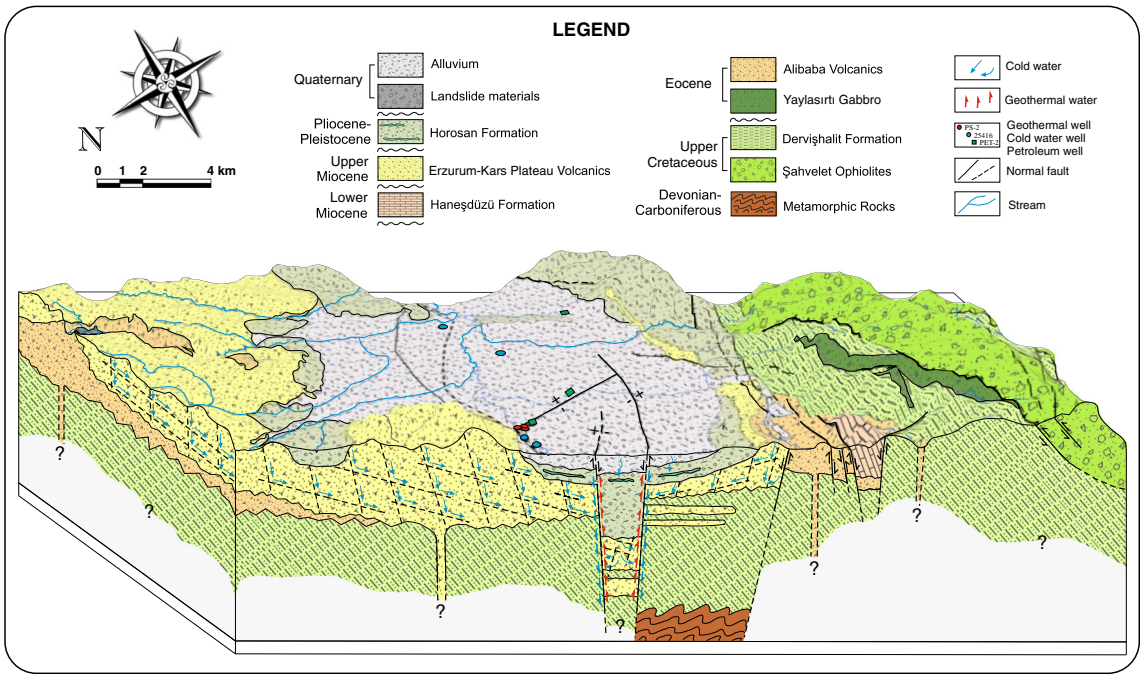

Fig. 14 Conceptual model of the Pasinler (Erzurum) geothermal field

Table 7 Chemistry of rocks in the study area (values are given as %)

Sample no.	R1	R2	ZB1	BB1	RT1
Lithology	Rhyolite	Rhyolite	Basalt	Basalt	Rhyolitic tuff
Formation name	Erz.-Kars Plt. Volc.	Erz.-Kars Plt. Volc.	Erz.-Kars Plt. Volc	Erz.-Kars Plt. Volc	Erz.-Kars Plt. Volc
Na_2O	5.35	5.32	3.53	3.44	4.71
MgO	0.23	0.09	5.57	5.70	0.41
Al_2O_3	15.21	15.18	16.98	18.01	15.38
SiO_2	69.65	70.59	54.17	52.49	67.25
P_2O_5	0.06	0.03	0.16	0.19	0.07
K_2O	5.01	5.04	1.52	0.99	4.92
CaO	0.62	0.45	8.33	8.65	1.52
TiO_2	0.24	0.15	1.07	1.12	0.40
Cr_2O_3	< 0.002	< 0.002	0.020	0.021	< 0.002
MnO	0.04	0.04	0.13	0.15	0.07
Fe_2O_3	2.58	2.09	7.40	7.59	1.91
LOI	0.8	0.8	0.8	1.3	3.1

Zouari et al. 2003; Goff and McMurtry 2010). Tritium values equal to or greater than 1 TU are acceptable as modern water; moreover, tritium concentrations below 1 TU show that groundwater is at least 50 years old. The tritium values below 0.8 TU indicate the system was recharged before the 1950s. In Fig. 11a, b, the tritium concentrations for all waters from Pasinler are plotted against EC and *T* values, respectively. The low TU high EC and T contents of the thermal waters indicate that these thermal waters have deeper circulating and longer residence times than the cold waters (except for JK cold spring). The low tritium value of the JK cold spring can be explained by deep circulation.

To determine the source of carbon and sulfur (SO_4) in the Pasinler waters, all water samples were analyzed for their $\delta^{13}C_{VPDB}$ (Versus Pee Dee Belemnite) and $\delta^{34}S_{CDT}$ (Canyon Diablo Troilite). The $\delta^{13}C$ (DIC) contents for Pasinler waters range from 8.13 to 9.54‰ for thermal waters, from − 7.14 to − 9.99‰ for cold spring, and from − 9.61 to +6.19‰ for surface waters (Table 6). These results indicate that carbon in the thermal waters originates from mainly groundwater DIC. Also, young volcanic rocks outcropping around the study area suggest that carbon in the waters originates from volcanic (mantle) CO_2. Carbon in the surface waters and cold spring (except for HD) has a negative carbon content. HD (surface water), which has thermal water discharges, has positive carbon values which are controlled by CO_2 in the soil and groundwater DIC (Clark and Fritz 1997). The $\delta^{13}C$ (DIC) contents are plotted vs. alkalinity for all water samples in Fig. 12. As a result, HCO_3 values of the geothermal waters show an enriched value of $\delta^{13}C$ with respect to the cold water spring.

$\delta^{34}S$ ‰VCDT values of SO_4 are in range 18.64 to 36.18‰ in geothermal waters (OZ, PS3 and HDK), 1.94‰ in cold water spring (JK), and 13.44 to 14.4‰ in surface waters (HD and HDE). These results are evaluated according to the diagram (Krouse 1980). The sources of the sulfur are volcanic origin sulfur, oil, coal, and limestone according to the data obtained from the PS3 geothermal well (Fig. 13). The economically important coal in the lower levels of the Horosan formation and oil that seeps around the geothermal springs and Erzurum-Kars plateau volcanics outcropping in a vast area also confirm the source of the sulfur in the Pasinler basin. According to the diagram of sulfur isotope distribution in nature (Krouse 1980), the sources of the sulfur are limestone, volcanic rocks, oil-coal, and cold and surface waters (JK, HD, HDE) too.

Conceptual model of the Pasinler geothermal field

The conceptual model of the Pasinler geothermal system has been evaluated using hydrogeology, hydrochemistry, and environmental isotope studies together with regional geological structure (Fig. 14). According to the deep drills (Pelin 1970, 1981), it is clear that there are metamorphic rocks at the basement, which are overlain by Upper Cretaceous sedimentary rocks (Derviş Halit formation). Sedimentary rocks at some areas are cut off by Upper Miocene young volcanic rocks (Erzurum-Kars plateau volcanics). Conglomerate and sandstone intercalated with marl (Horosan formation) and alluvium form the cap rock in the basin. The compression regime along the N–S direction (Yılmaz et al. 1989) and strike–slip faults have caused volcanic activities north of the basin (Aynalı and Bulut 2002). At the north of the basin, dome structures of different rock types and fissure-type volcanism have occurred (Keskin et al. 1998). These volcanic rocks in the basin are basalt, andesite, dacite, rhyodacite, rhyolite, and ignimbrite. The geothermal boreholes drilled by MTA indicate that the reservoir rock is basalt and basaltic tuff at deep, and rhyolite and rhyolitic tuff at upper levels. Geothermometer calculations and isotope geochemistry studies indicate that a low temperature and meteoric origin

Table 8 Trace element compositions of the rocks from the study area (μg/L)

Elements	Co	Ni	Cu	Zn	Ga	As	Se	Rb	Sr	Y	Zr	Nb	Mo	Cd	Sn	Sb	Cs	Ba	La	Ce	Hf	Ta	W	Hg	Tl	Pb	Th	U
R1	1.0	1.8	3.5	64	20.7	0.5	0.5	112.1	41.6	44.2	427.2	28.1	3.2	0.1	7	0.1	3.7	870	68.0	114.7	9.6	1.5	7.9	0.01	0.1	4.0	16.5	5.0
R2	0.5	0.6	3.3	83	20.4	1.0	1.0	120.3	18.7	43.4	367.0	31.5	3.2	0.1	5	0.1	2.5	498	82.1	133.8	9.6	2	1.3	0.01	0.1	5.5	19.6	5.6
ZB1	31.9	50.4	29.2	36	18.3	0.5	0.5	37.9	433.2	22.3	188.5	11.7	1.3	0.1	2	0.1	1.0	362	26.2	49.8	3.7	0.6	0.7	0.01	0.1	0.9	7.4	1.7
BB1	31.2	69.2	22.0	41	19	0.5	0.5	19.4	458.0	25.5	187.7	11.1	1.0	0.1	2	0.1	0.6	549	35.0	56.1	4.3	0.7	0.7	0.01	0.1	4.0	7.3	1.6
RT1	1.3	3.6	2.8	64	17.5	0.5	0.5	119.4	149.6	28.7	468.0	24.3	0.9	0.1	3	0.1	3.5	884	54.8	93.2	10.5	1.6	2.4	0.01	0.1	1.2	23.4	6.1

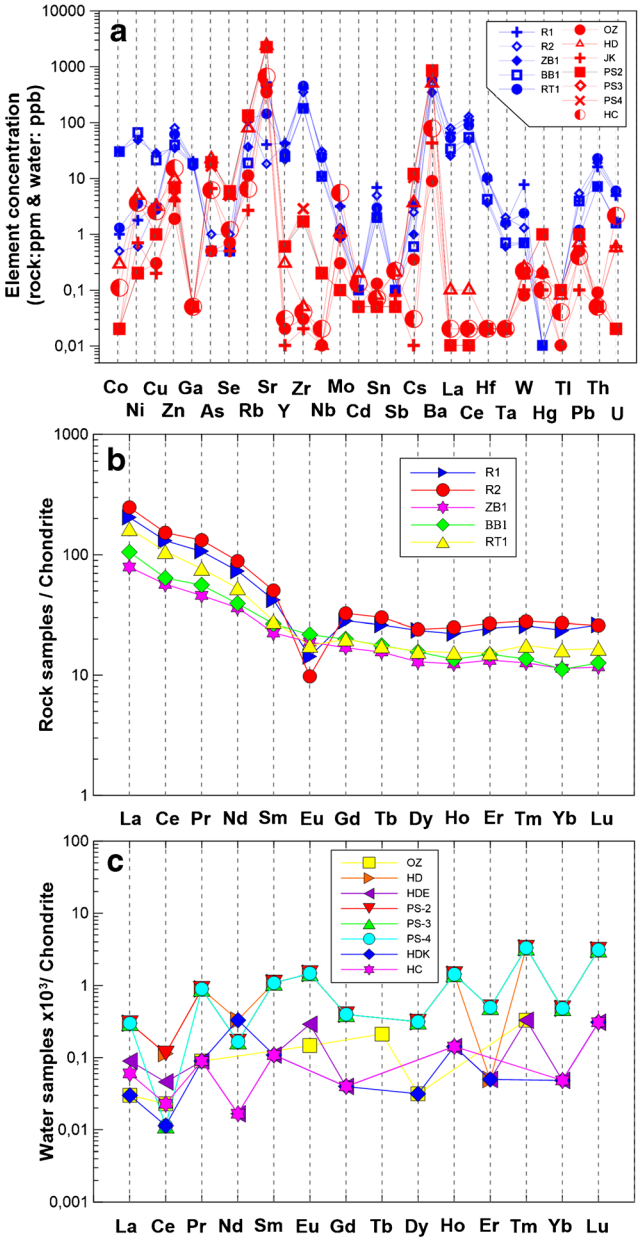

Fig. 15 Distribution of trace element for rocks and waters (**a**), chondrite-normalized REE patterns of rocks (Haskin et al., 1968) (**b**), and waters (Evens et al., 1978) from the Pasinler (Erzurum) geothermal field in Turkey (**c**)

geothermal system. Precipitation in the basin is filtered to depth along the faults and fractures and it is heated in the temperature anomaly field. The magma that formed the young volcanics (Erzurum-Kars plateau volcanics) is the main heat source of the geothermal system in the Pasinler geothermal field. Hydrochemical and isotope contents in the geothermal waters show different degrees of mixing with cold groundwater before rising to the surface. Silty and marl levels of the Horosan formation and clayey levels of alluvium are the cap rock of the system.

Table 9 REE analytical results of spring and rock samples (concentration in ppb for springs and ppm for rock samples)

		La	Ce	Pr	Nd	Sm	Eu	Gd	Tb	Dy	Ho	Er	Tm	Yb	Lu
	R1	68.0	114.7	11.95	44.0	7.70	0.98	7.12	1.23	7.46	1.55	4.94	0.77	4.89	0.85
Rock	R2	82.1	133.8	14.83	53.3	9.20	0.67	8.20	1.42	7.61	1.74	5.43	0.84	5.60	0.84
	ZB1	26.2	49.8	5.13	21.7	4.12	1.29	4.27	0.73	4.10	0.87	2.68	0.38	2.35	0.38
	BB1	35.0	56.1	6.27	23.5	4.87	1.49	5.02	0.83	4.96	0.95	3.00	0.41	2.32	0.41
	RT1	54.8	93.2	8.58	31.6	5.13	1.21	5.03	0.82	5.00	1.08	3.08	0.53	3.37	0.54
	OZ	0.01	0.02	0.01	0.01	0.02	0.01	0.01	0.01	0.01	0.01	0.01	0.01	0.01	0.01
Waters	HD	0.1	0.1	0.1	0.2	0.2	0.1	0.1	0.1	0.1	0.1	0.01	0.1	0.1	0.1
	HDE	0.03	0.04	0.01	0.01	0.02	0.02	0.01	0.01	0.01	0.01	0.01	0.01	0.01	0.01
	PS-2	0.1	0.1	0.1	0.1	0.2	0.1	0.1	0.1	0.1	0.1	0.1	0.1	0.1	0.1
	PS-3	0.1	0.01	0.1	0.1	0.2	0.1	0.1	0.1	0.1	0.1	0.1	0.1	0.1	0.1
	PS-4	0.1	0.01	0.1	0.1	0.2	0.1	0.1	0.1	0.1	0.1	0.1	0.1	0.1	0.1
	HDK	0.01	0.01	0.01	0.2	0.02	0.01	0.01	0.01	0.01	0.01	0.01	0.01	0.01	0.01
	HC	0.02	0.02	0.01	0.01	0.02	0.01	0.01	0.01	0.01	0.01	0.01	0.01	0.01	0.01

Rock geochemistry

The different rock types (basalt, rhyolite, and rhyolitic tuff) outcropping in the Pasinler geothermal area were analyzed to compare with the water and rock geochemistry (Table 7). The chemistry of the surrounding rocks shows that the most abundant oxides are SiO_2 and Al_2O_3, respectively. The trace element concentrations of the sampled rocks (basalt, rhyolite, and rhyolitic tuff) in the study area are given in Table 8. According to the analysis results, while trace elements such as Ba, Sr, Rb, Zr, Ce, Zn, and Ga have high concentrations, the elements such as Se, Cd, Sn, Sb, and Hg have low concentrations. The samples from the water and rock are similar in their Sr, Ba, Rb, and Zn content. Since magmatic–volcanic rocks have clearly the highest Ba and Sr elements (Hem 1970), the high concentrations of Ba and Sr in the water indicate that this element originated from rhyolite, rhyolitic tuff and basalt and water–rock interaction in the study area (Fig. 15a).

Rare earth elements and water–rock interaction

In addition to the major elements in the geothermal waters, the rare earth elements (REE) can be used in the investigation of water–rock interaction and exploration for geothermal resources (Smedley 1991; Lewis et al. 1997, 1998; Wood and Shannon, 2003; Sanada et al. 2006; Gammons et al. 2005, Göb et al. 2013, Shakeri et al. 2015). REE content in the volcanic rocks and all water samples were analyzed in the Pasinler basin and are reported in Table 9. The chondrite-normalized (Haskin et al. 1968) REE distribution of the rocks in the study area shows variable enrichment in light REE (LREE) compared to heavy REE (HREE) and negative Eu anomalies (Fig. 15b). This is typical of the upper continental crust (McLennan 1989). The low concentrations of REE were observed in the waters (Fig. 15c).The chondrite-normalized (Evens et al. 1978) REE patterns of the waters are different from those of the rocks; LREE are slightly depleted relative to the HREE and have negative Ce anomalies and positive Eu anomalies which indicate oxygen-rich environments (Constantopoulos 1988).

Water–rock interaction was evaluated according to Hounslow (1995) and was simulated in the computer program Aquachem 2012.2. The different ionic comparisons of Hounslow 1995 and the calculated results in this study are shown in Table 10. According to these results, the $(Na^+ + K^+ - Cl^-)/(Na^+ + K^+ - Cl^- + Ca^{2+})$ ratios of all the water samples are > 0.2 and < 0.8, indicating plagioclase weathering is possible. The ratio of $Na^+/(Na^+ + Cl^-)$ is > 0.5 for all waters (except for HDK) and 0.5 for HDK, indicating a sodium source other than halit–albite, ion exchange, and halite solution, respectively (Hounslow 1995). The ratio of $Mg^{2+}/(Ca^{2+} + Mg^{2+})$ is < 0.5 for PS-2, PS-3, PS-4, HC, HD, and HDE; 0.5 for OZ; and > 0.5 for HDK, and JK, while the situation of $HCO^{3-}/SiO^2 > 10$ is indicating limestone–dolomite weathering, dolomite weathering and dolomite dissolution, and calcite precipitation, respectively. The $Ca^{2+}/(Ca^{2+} + SO_4^{2-})$ ratios were found to be > 0.5, showing a calcium source other than gypsum, carbonate, or silicate. The $SiO_2/(Na^+ + K^+ + Cl^-)$ ratio is < 1 in the examined waters, indicating cation exchange. The source of Cl^- ions is weathering of the rocks (Hounslow 1995). The HCO_3^-/ anion ratio is < 0.8 for HDK, PS-2, PS-3, and PS-4 and > 0.8 for OZ, JK, HC, HD, and HDE, showing seawater and brine, and silicate or carbonate weathering, respectively (Hounslow 1995).

Table 10 Water–rock interaction processes in the investigated waters (Hounslow, 1995)

Parameter	HDK	PS-2	PS-3	PS-4	OZ
$(Na^+ + K^+ - Cl^-)/(Na^+ + K^+ - Cl^- + Ca^{2+})$	0.014 Plagioclase weathering unlikely	0.39 Plagioclase weathering possible	0.46 Plagioclase weathering possible	0.60 Plagioclase weathering possible	0.29 Plagioclase weathering possible
$Na^+/(Na^+ + Cl^-)$	0.50 Halite solution	0.54 Sodium source other than halit–albite, ion exchange	0.56 Sodium source other than halit–albite, ion exchange	0.59 Sodium source other than halit–albite, ion exchange	0.79 Sodium source other than halit–albite, ion exchange
$Mg^{2+}/(Ca^{2+} + Mg^{2+})$	0.52 Dolomite weathering	0.41 Limestone–dolomite weathering	0.37 Limestone–dolomite weathering	0.40 Limestone–dolomite weathering	0.50 Dolomite dissolution, calcite precipitation, or seawater
$Ca^{2+}/(Ca^{2+} + SO_4^{2-})$	0.99 Calcium source other than gypsum-carbonates or silicates	0.99 Calcium source other than gypsum-carbonates or silicates	0.99 Calcium source other than gypsum-carbonates or silicates	0.99 Calcium source other than gypsum-carbonates or silicates	0.99 Calcium source other than gypsum-carbonates or silicates
$SiO_2/(Na + K + Cl)$	− 7.4 Cation exchange	0.18 Cation exchange	0.13 Cation exchange	0.08 Cation exchange	0.49 Cation exchange
Cl^-/ anions	0.30 Rock weathering	0.53 Rock weathering	0.49 Rock weathering	0.47 Rock weathering	0.05 Rock weathering
HCO_3^-/ anions	0.64 Seawater or brine	0.44 Seawater or brine	0.48 Seawater or brine	0.51 Seawater or brine	0.93 Silicate or carbonate weathering
Calcite SI	0.45 Oversaturated calcite	− 0.7 Undersaturated calcite	− 0.48 Undersaturated calcite	− 0.8 Undersaturated calcite	− 0.53 Undersaturated with respect to calcite

Parameter	JK	HC	HD	HDE
$(Na^+ + K^+ - Cl^-)/(Na^+ + K^+ - Cl^- + Ca^{2+})$	0.21 Plagioclase weathering possible	0.14 Plagioclase weathering possible	0.21 Plagioclase weathering possible	0.10 Plagioclase weathering possible
$Na^+/(Na^+ + Cl^-)$	0.89 Sodium source other than halit–albite, ion exchange	0.79 Sodium source other than halit–albite, ion exchange	0.78 Sodium source other than halit–albite, ion exchange	0.75 Sodium source other than halit–albite, ion exchange
$Mg^{2+}/(Ca^{2+} + Mg^{2+})$	0.53 Dolomite dissolution, calcite precipitation, or seawater	0.42 Limestone–dolomite weathering	0.47 Limestone–dolomite weathering	0.46 Limestone-Dolomite weathering
$Ca^{2+}/(Ca^{2+} + SO_4^{2-})$	0.91 Calcium source other than gypsum-carbonates or silicates	0.92 Calcium source other than gypsum-carbonates or silicates	0.98 Calcium source other than gypsum-carbonates or silicates	0.96 Calcium source other than gypsum-carbonates or silicates
$SiO_2/(Na + K + Cl)$	0.39 Cation exchange	0.63 Cation exchange	0.45 Cation exchange	0.92 Cation exchange
Cl^-/ anions	0.01 Rock weathering	0.03 Rock weathering	0.04 Rock weathering	0.02 Rock weathering
HCO_3^-/ anions	0.94 Silicate or carbonate weathering	0.93 Silicate or carbonate weathering	0.93 Silicate or carbonate weathering	0.95 Silicate or carbonate weathering
Calcite SI	− 2.33 Undersaturated with respect to calcite	− 2.3 Undersaturated with respect to calcite	− 0.59 Undersaturated with respect to calcite	− 1.09 Undersaturated with respect to calcite

The decomposition reactions of kaolinite decomposition of silicates such as albite, anorthite, and K-feldspar are given by Eqs. (1–3) (Appelo and Postma, 1994) and decomposition reactions of carbonates are given by Eq. (4).

$$\underset{\text{Albite}}{2NaAlSi_3O_8} + 2H^+ + 9H_2O \rightarrow \underset{\text{Kaolinite}}{Al_2Si_2O_5(OH)_4} + 2Na^+ + 4\,H_4SiO_4 \quad (1)$$

$$\underset{\text{Anorthite}}{2CaAl_2Si_2O_8} + 2H^+ + H_2O \rightarrow Al_2Si_2O_5(OH)_4 + 2Ca^{2+} \quad (2)$$

$$\underset{\text{K-feldspar}}{2KAlSi_3O_8} + 2H^+ + 9H_2O \rightarrow Al_2Si_2O_5(OH)_4 + 2K^+ + 4H_4SiO_4 \quad (3)$$

$$\underset{\text{Calcite}}{CaCO_3} + H_2CO_3 \rightarrow Ca^{2+} + 2HCO_3^- \quad (4)$$

Conclusions

The Pasinler basin has been formed because of the compression regime along N–S direction caused by sinistral strike–slip faults at E–W direction. It is accepted that the volcanic domes at the north and south of the basin have been formed because of this regime. The geothermal system is associated with the Erzurum-Kars Plate volcanic rocks. Na–Cl–HCO_3-type geothermal liquid is of meteoric origin based on isotope composition. The heat transfer in the system occurs with convective transportation. Both hydrogeochemical properties and isotopic composition of the waters indicate that the hot waters rising from the geothermal reservoir via faults mix with ground waters coming from the shallow cold water aquifer before surfacing. The temperatures measured at the geothermal borehole (51 °C) and the temperatures calculated according to silica geothermometers show that the geothermal system has a low enthalpy. The tritium values below 0.8 TU in geothermal waters indicate the system was recharged before the 1950s.

Based on the trace element concentration, it is seen that the water chemistry is affected by the chemistry of the volcanic rocks which form the geothermal reservoir. The major ions (Ca, K, Na) in the geothermal water originated from the weathering of plagioclase and cation exchange.

Acknowledgements We are grateful to Assistant Prof. Arzu Fırat Ersoy for assistances in the fieldwork. The authors also thank Assistant Prof. Adam Milewski from the University of Georgia (USA) for his help with the English of the final text.

Funding information This research was supported by the Karadeniz Technical University Research Project Fund (Project Number: 1063).

References

Akkus I, Akıllı H, Ceyhan S, Dilemre A, Tekin Z (2005) Turkiye Jeotermal Kaynakları Envanteri, Maden Tetkik Arama Genel Mudurlugu Envanter Serisi-201 Ankara (in Turkish)

APHA (American Public Health Association), AWWA (American Water Work Association) and WPCF (Water Pollution Control Federation) (1995) Standard methods for the determination of water and waste water, 15th edn. APHA, Washington, DC

Appelo CAJ, Postma D (1994) Geochemistry, groundwater and pollution. Balkema, Rotterdam, p 536

Arnorsson S (1983) Chemical-equilibria in icelandic geothermal systems-implications for chemical geothermometry investigations. Geothermics 12(2–3):119–128. https://doi.org/10.1016/0375-6505(83)90022-6

Aravena R, Mayer B (2009) Isotopes and processes in the nitrogen and sulfur cycles. In: Aelion CM, Höhener P, Hunkeler D, Aravena R (eds) Environmental isotopes in biodegradation and bioremediation. CRC Press, Boca Raton, pp 203–246. https://doi.org/10.1201/9781420012613.ch7

Aydın H, Ekmekçi M, Tezcan L, Dişli E, Aksoy L, Yalçın MP, Özcan G (2009). Assessment of water resources potential of Gürpınar (Van) Karst Springs with regard to sustainable management. TUBITAK project (no. 106Y040), final report (in Turkish)

Aynalı Z, Bulut H (2002) Pasinler (Erzurum) Belediyesi Jeotermal Ön Etüt Raporu, Ankara (in Turkish) (unpublished)

Baba A, Sanliyuksel D (2011) Hydrogeochemical and isotopic composition of a low-temperature geothermal source in northwest Turkey: case study of Kirkgecit geothermal area. Environ Earth Sci 62:529–540

Berner ZA, Stuben D, Leosson MA, Klinge H (2002) S- and O-isotopic character of dissolved sulphate in the cover rock aquifers of a Zechstein salt dome. Appl Geochem 17(12):1515–1528. https://doi.org/10.1016/S0883-2927(02)00046-X

Bundschuh J, Maity JP, Nath B, Baba A, Gunduz O, Kulp TR, Jean JS, Kar S, Tseng Y, Bhattacharya P, Chen CY (2013) Naturally occurring arsenic in terrestrial geothermal systems of western Anatolia, Turkey: potential role in contamination of freshwater resources. J Hazard Mater 262:951–959. https://doi.org/10.1016/j.jhazmat.2013.01.039

Bureau of Reclamation (Reclamation) (1995) Ground water manual, a water resources technical publication, for sale by the Superintendent of Documents. U.S. Government Printing Office, Washington DC

Calmbach L (1997) AquaChem computer code-version 3.7.42. Waterloo Hydrogeologic, Waterloo, ON

Canfield DE (2001) Isotope fractionation by natural populations of sulfate-reducing bacteria. Geochim Cosmochim Acta 65(7):1117–1124. https://doi.org/10.1016/S0016-7037(00)00584-6

Clark ID, Fritz P (1997) Environmental isotopes in hydrogeology. CRC Press/Lewis, Boca Raton, p 328

Craig H (1961) Isotopic variations in meteoric waters. Science 133(3465): 1702–1703. https://doi.org/10.1126/science.133.3465.1702

Constantopoulos J (1988) Fluid inclusion and rare earth element geochemistry of fluorite from south-central Idaho. Econ Geol 83(3): 626–636. https://doi.org/10.2113/gsecongeo.83.3.626

Delalande M, Bergonzini L, Gherardi F, Guidi M, Andre L, Abdallah I, Williamson D (2011) Fluid geochemistry of natural manifestations from the southern Poroto-Rungwe hydrothermal system (Tanzania): preliminary conceptual model. J Volcanol Geotherm Res 199(1-2): 127–141. https://doi.org/10.1016/j.jvolgeores.2010.11.002

Deutsch WJ (1997) Groundwater geochemistry: fundamentals and application to contamination. Lewis publisher, USA

Dilek R (1973). Mathematical modeling of the aquifers, application of Pasinler (Erzurum) and Çamlıbel (Tokat) Basin, İstanbul University. Associate Professor thesis (in Turkish-unpublished)

Evens NM, Hamilton PJ, O'Nions RK (1978) Rare earth abundances in chondritic meteorite. Geochim Cosmochim Acta 42(8):1199–1212. https://doi.org/10.1016/0016-7037(78)90114-X

Fırat-Ersoy A, Sönmez SÇ (2014) Hydrogeochemical and isotopic characteristics of the Ilica geothermal system (Erzurum, Turkey). Environ Earth Sci 72(11):4451–4462. https://doi.org/10.1007/s12665-014-3345-z

Filiz Ş, (1982) Ege Bölgesindeki Önemli Jeotermal alanların ^{18}O, ^{2}H, ^{3}H, ^{13}C izotoplarıyla incelenmesi (in Turkish). Assoc. Prof. Thesis. E.Ü.Y.B.F., İzmir

Fontes JC (1980) Environmental isotopes in groundwater hydrology. In: Fritz P, Fontes JC (eds) Handbook of environmental isotope geochemistry, the terrestrial environment, 1A. Elsevier, Amsterdam, pp 75–140

Fournier RO (1977) Chemical geothermometers and mixing models for geothermal systems. Geothermics 5(1-4):41–50. https://doi.org/10.1016/0375-6505(77)90007-4

Fournier RO (1979) Geochemical and hydrologic considerations and the use of enthalpy-chloride diagrams in the prediction of underground conditions in hotspring systems. J Volcanol Geoth Res. 5(1–2):1–16. https://doi.org/10.1016/0377-0273(79)90029-5

Freeze RA, Cherry JA (1979) Groundwater. Prentice-Hail, USA, p 604

Gammons CH, Wood SA, Pedrozo F, Varekamp JC, Nelson BJ, Shope CL, Baffico G (2005) Hydrogeochemistry and rare earth element behavior in a volcanically acidified watershed in Patagonia, Argentina. Chem Geol 222(3-4):249–267. https://doi.org/10.1016/j.chemgeo.2005.06.002

Gat JR, Carmi I (1970) Evolution of the isotopic composition of atmospheric waters in the Mediterranean Sea area. J Geophys Res 75(15):3039–3048. https://doi.org/10.1029/JC075i015p03039

Gemici U, Filiz S (2001) Hydrochemistry of the Cesme geothermal area in western Turkey. J Volcanol Geotherm Res 110(1-2):171–187. https://doi.org/10.1016/S0377-0273(01)00202-5

Giggenbach WF (1988) Geothermal solute equilibria-derivation of Na-K-Mg-Ca geoindicators. Geochim Cosmochim Acta 52(12):2749–2765. https://doi.org/10.1016/0016-7037(88)90143-3

Giggenbach WF (1991) Chemical techniques in geothermal exploration,: in Applications of geochemistry in geothermal reservoir development, UNITAR-UNDP (ed. F. D'Amore), 119–144

Goff F, McMurtry GM (2000) Tritium and stable isotopes of magmatic waters. J Volcanol Geotherm Res 97(1-4):347–396. https://doi.org/10.1016/S0377-0273(99)00177-8

Göb S, Loges A, Nolde N, Bau M, Jacob DE, Markl G (2013) Major and trace element compositions (including REE) of mineral, thermal, mine and surface waters in SW Germany and implications for water–rock interaction. Appl Geochem 33:127–152. https://doi.org/10.1016/j.apgeochem.2013.02.006

Gulec N (1988) The distribution of helium-3 in western Turkey. Miner Res Explor Bull 108:35–42

Gultekin F, Hatipoglu E, Fırat Ersoy A (2011) Hydrogeochemistry, environmental isotopes and the origin of the Hamamayagı-Ladik thermal spring (Samsun, Turkey). Environ Earth Sci 62:1351–1360

Haskin LA, Wildeman TR, Haskin MA (1968) An accurate procedure for the determination of the rare earths by neutron activation. J Radioanal Chem 1(4):337–348. https://doi.org/10.1007/BF02513689

Hem JD (1970). Study and interpretation of the chemical characteristics of natural water. Water-supply paper - Geological Survey (U.S.), Second Edition, 1473, 363

Hounslow AW (1995). Water quality data: analysis and interpretation, Lewis Publishers, 54

IAH (International Association of Hydrogeologist) (1979) Map of mineral and thermal water of Europe. Scale 1:500,000. International Association of Hydrogeologist

Karakus H, Simsek S (2013) Tracing deep thermal water circulation systems in the E-W trending Büyük Menderes Graben, western Turkey. J Volcanol Geotherm Res 252:38–52. https://doi.org/10.1016/j.jvolgeores.2012.11.006

Keskin M, Pearce JA, Mitchell JG (1998) Volcano-stratigraphy and geochemistry of collision-related volcanism on the Erzurum-Kars plateau, North Eastern Turkey. J Volcanol Geotherm Res 85(1-4):355–404. https://doi.org/10.1016/S0377-0273(98)00063-8

Kharaka YK, Mariner RH (1989) Chemical geothermometers and their application to formation waters from sedimentary basins. In: Naser ND, McCollin TH (eds) Thermal history of sedimentary basin. Springer-Verlag, New York, pp 99–117. https://doi.org/10.1007/978-1-4612-3492-0_6

Krouse HR (1980) Sulphurv isotopes in our environment. In: Fritz P, Fontes J-C (eds) Handbook of environmental isotope geochemistry I, the terrestrial environment. A. Elsevier, Amsterdam, The Netherlands, pp 435–472

Lewis AJ, Palmer MR, Sturchio NC, Kemp AJ (1997) The rare earth element geochemistry of acid-sulphate and acid-sulphate-chloride geothermal systems from Yellowstone National Park, Wyoming, USA. Geochim Cosmochim Acta 61(4):695–706. https://doi.org/10.1016/S0016-7037(96)00384-5

Lewis AJ, Komninou A, Yardley BWD, Palmer MR (1998) Rare earth element speciation in geothermal fluids from Yellowstone National Park, Wyoming, USA. Geochim Cosmochim Acta 62(4):657–663. https://doi.org/10.1016/S0016-7037(97)00367-0

Lund JW, Freeston DH, Boyd TL (2010) Direct application of geothermal energy: 2010 worldwide review. Geothermics 40:159–180

Ma R, Wang Y, Sun Z, Zheng C, Ma T, Prommer H (2011) Geochemical evolution of groundwater in carbonate aquifers in Taiyuan, northern China. Appl Geochem 26(5):884–897. https://doi.org/10.1016/j.apgeochem.2011.02.008

Magri F, Akar T, Gemici U, Pekdeger A (2010) Deep geothermal groundwater flow in the Seferihisar-Balçova area, Turkey: results from transient numerical simulations of coupled fluid flow and heat transport processes. Geofluids 10(3):388–405. https://doi.org/10.1111/j.1468-8123.2009.00267.x

Magana BMI (1999) Geochemical interpretation of thermal fluid discharge from wells and springs in the Berlín geothermal field, El Salvador. Report 7:165–191

McLennan SM (1989). Rare earth elements in sedimentary rocks: influence of provenance and sedimentary processes, in: Lipin, B.R. & McKay, G.A. (eds) Geochemistry and mineralogy of rare earth elements. Mineralogical Society of America, Reviews in Mineralogy, 21, 169–200

Miao Z, Brusseau ML, Carroll KC, Carreon-Diazconti C, Johnson B (2012) Sulfate reduction in groundwater: characterization and applications for remediation. Environ Geochem Health 34(4):539–550. https://doi.org/10.1007/s10653-011-9423-1

Mutlu H (2007) Constraints on the origin of the Balıkesir thermal waters (Turkey) from stable isotope (δ18O, δD, δ13C, δ34S) and major-trace element compositions. Turk J Earth Sci 16:13–32

Parkhurst D, Appelo CAJ (1999) User's guide to PHREEQC (Version 2)-A computer program for speciation, batch-reaction, onedimensional transport and inverse geochemical calculations. USGS Water Resources Investigation Report 99–4259

Pasvanoglu S, Gultekin F (2012) Hydrogeochemical study of the Terme and Karakurt thermal and mineralized waters from Kirsehir Area, Central Turkey. Environ Earth Sci 66(1):169–182. https://doi.org/10.1007/s12665-011-1217-3

Pasvanoglu S (2013) Hydrogeochemistry of thermal and mineralized waters in the Diyadin (Agri) area, eastern Turkey. Appl Geochem 38:70–81. https://doi.org/10.1016/j.apgeochem.2013.08.010

Pelin S (1970). Pasinler-2 kuyu bitirme raporu. MTA Rap.No: 4532. Yayımlanmamış

Pelin S (1981) Explanation of main rock properties and genesis of oil in the Pasinler basin. Earth Sci J Karadeniz Tech Univ 1:127–142

Piper AM (1944) A graphic procedure in the geochemical interpretation of water analyses. Am Geophys Union Trans 25:914–923

Shakeri A, Ghoreyshinia S, Mehrabi B, Delavari M (2015) Rare earth elements geochemistry in springs from Taftan geothermal area SE Iran. J Volcanol Geotherm Res 304:49–61. https://doi.org/10.1016/j.jvolgeores.2015.07.023

Simsek S (1982) Geology, geochemistry, and geothermal model of the Kizildere geothermal field. First Turkish-Italian Seminar on Geothermal Energy, Turkey, pp 1–25

Simsek S (1997) Geothermal potential in northwestern Turkey. Active tectonics of northwestern Anatolia. In: Schindler C, Pfister M (eds) The Marmara Poly-Project. vdf hochschulverlag AG an der ETH, Zurich, pp 111–123

Sungurlu O (1971). 1/50 000 ölçekli I47 a Paftasının Jeolojisi, TPAO Arama Grubu Başkanlığı, Jeoloji Arşivi, Ankara (in Turkish) (unpublished)

Sanada T, Takamatsu N, Yoshiike Y (2006) Geochemical interpretation of long-term variations in rare earth elements concentrations in acidic hot spring waters from the Tamagawa geothermal area, Japan. Geothermics 35(2):141–155. https://doi.org/10.1016/j.geothermics.2006.02.004

Smedley PL (1991) The geochemistry of rare earth elements in groundwater from the Carnmenellis area, southwest England. Geochim Cosmochim Acta 55(10):2767–2779. https://doi.org/10.1016/0016-7037(91)90443-9

Şengör AMC (1980) Türkiye'nin Neotektoniğinin Esasları (fundamentals of the neotectonics of Turkey), Publication of Geological Society of Turkey, p 40

Tarcan G (2002) Geothermal water chemistry, centre of geothermal energy. Research and Application (Jenarum), Summer School Publications, 87–113 (in Turkish)

Tarcan G, Gemici U (2003) Water geochemistry of the Seferihisar geothermal area, Izmir, Turkey. J Volcanol Geotherm Res 126(3-4): 225–242. https://doi.org/10.1016/S0377-0273(03)00149-5

Tarcan G (2005) Mineral saturation and scaling tendencies of waters discharged from wells (N150 8C) in geothermal areas of Turkey. J Volcanol Geotherm Res 142:263–283

Truesdell AH, Fournier RO (1977) Procedure for estimating the temperature of a hot water component in a mixed water by using a plot of dissolved silica versus enthalpy. USGS J Res 5:49–52

Verma SP, Santoyo E (1997) New improved equations for Na/K, Na/Li and SiO_2 geothermometers by outlier detection and rejection. J Volcanol Geoth Res 79(1–2):9–23. https://doi.org/10.1016/S0377-0273(97)00024-3

Wood SA, Shannon WM (2003) Rare-earth elements in geothermal waters from Oregon, Nevada, and California. Solid State Chem 171(1-2):246–253. https://doi.org/10.1016/S0022-4596(02)00160-3

Yılmaz A, Terlemez I, Uysal Ş (1989) 1/100 000 ölçekli Türkiye Jeoloji Haritaları Serisi Erzurum F-33 Paftası. M.T.A, Ankara (in Turkish)

Yılmazer S (2001) Kıyı Ege ve İzmir İli'ndeki Jeotermal kaynakların değerlendirilmesi. Yer altı Suları ve Çevre Sempozyumu, 21-23 Mart 2001. Bildiriler, İzmir, pp 371–379 (In Turkish)

Yuce G, Taskiran L (2013) Isotope and chemical compositions of thermal fluids at Tekman geothermal area (eastern Turkey). Geochem J 47(4):423–435. https://doi.org/10.2343/geochemj.2.0262

Zuari K, Hkir N, Ouda B (2003) Palaeoclimatic variation in Maknassi basin (central Tunisia) during Holocene period using pluridisplinary approaches. Tech Doc IAEA Vienna 2:80–88